Journal of Materials Chemistry A

Accepted Manuscript

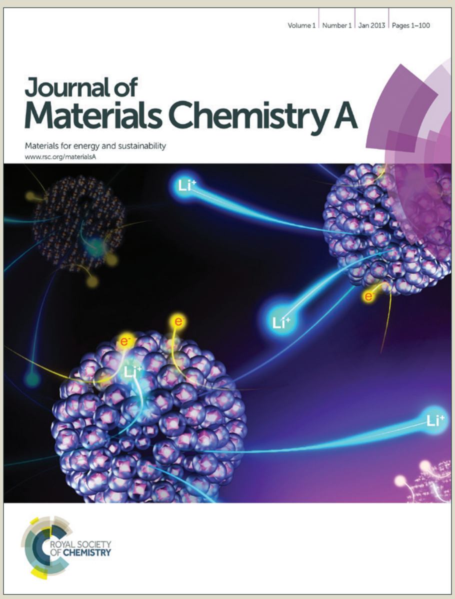

Journal of Materials Chemistry A

Cite this: DOI: 10.1039/c0xx00000x

www.rsc.org/xxxxxx

ARTICLE TYPE

Porous $MnFe_2O_4$ Microrods as Advanced Anodes for Li-ion Batteries with Long Cycle Lifespan

Nana Wang,[a] Xiaojian Ma,[a] Yunpo Wang,[a] Jian Yang[a] and Yitai Qian*[a,b]

Received (in XXX, XXX) Xth XXXXXXXXX 20XX, Accepted Xth XXXXXXXXX 20XX
DOI: 10.1039/b000000x

Abstract: Porous electrode materials with both high rate capabilities and long cycle lives are significant to satisfy the urgent demand of energy storage. Furthermore, one dimensional structure can facilitate Li^+ diffusion and accommodate the volume expansion. Here, porous $MnFe_2O_4$ microrods have been successfully synthesized by a room temperature reaction and then moderate annealing in Ar atmosphere. The porous $MnFe_2O_4$ electrodes exhibit high reversible capacity and outstanding cycling stability (after 1000 cycles still keep about 630 mAh g^{-1} at the current density of 1 A g^{-1}), as well as a high coulombic efficiency (> 98%). Moreover, even at a high current density 4 A g^{-1}, the porous $MnFe_2O_4$ microrods can still maintain a reversible capacity of 420 mAh g^{-1}. These results demonstrate that the porous $MnFe_2O_4$ microrods are promising anode materials for high performance Li-ion batteries.

Introduction

Rechargeable lithium ion batteries (LIBs), as a ubiquitous power sources, have been widely used in portable devices.[1] Recently, numerous applications such as electric vehicles are calling for improvement in terms of power and energy density of LIBs. Presently, graphite, as dominant anode material for commercial LIBs, exhibits a low theoretical capacity (375mAh g^{-1}) and safety drawbacks due to its low reaction voltage.[2,3] Therefore, much efforts have been made to search for alternative anode materials to match the needs of high energy storage and long cycling stability. Transition metal oxides as potential substitutes offering at least twice the capacity of graphite have been widely studied.[3-5] As one of the binary metal oxides, $MnFe_2O_4$ have attracted much attention due to its high theoretical capacity (926 mAh g^{-1}), environmental benignity and low cost.[6-10] However, $MnFe_2O_4$ suffers from large volume change during lithiation/delithiation and low Li^+ diffusion coefficient, resulting in low coulombic efficiency and poor cycling stability.

Designing nano/microsized structures is one effective strategy to overcome the above issues.[3,4] Among various structures, microrods can provide short and continuous diffusion path for electron/ion transfer, which have been proved in experiment.[11-13] In addition, creating pores on microrods not only can prevent the pulverization of active materials, but also can accommodate the volume change during cycling. Moreover, the pores can enlarge the surface area and provide good access of the electrolyte to the electrode surface.[14-16] Thus, employing one dimensional in combination with porous structured electrodes is a valid way to benefit the LIBs including long-term stability and high rate performance. To our knowledge, there are a few reports to explore $MnFe_2O_4$ applied as an anode material. Su *et al* synthesized mesoporous $MnFe_2O_4$ microspheres, which maintains 678.6 mAh g^{-1} at a current density of 185.6 mA g^{-1} only after 50 cycles.[6] Furthermore, $MnFe_2O_4$/graphene nanocomposites have already been prepared presenting improved cycling stability, which is attributed to the excellent electronic conductivity of graphene.[7-9] Despite the progress has been made, there are still some shortcomings such as poor rate capacity and capacity fading during long-term cycling. Meanwhile, the synthesis method of composite material is a bit complicated. So there is still large room to improve its electrochemical properties.

In the present work, porous $MnFe_2O_4$ microrods were successfully synthesized using a microemulsion-based method following by a calcinations process. Here, Mn^{2+} and Fe^{2+} linked to $C_2O_4^{2-}$ to form a solid precipitation $Mn_xFe_{1-x}(C_2O_4)_2$ with the existence of surfactant. The precursor transformed into porous $MnFe_2O_4$ microrods after calcination in Ar atmosphere. The electrochemical performance of $MnFe_2O_4$ microrods was systematically investigated. The structural features, involving one dimensional structure can facilitate the ion/electron transfer, as well as plenty pores can tolerate volume changes during cycling process and enlarge the contacting area between electrolyte and electrode, which would benefit the electrochemical performance of porous $MnFe_2O_4$ microrods. Hence, the sample exhibits superior power rate capability and ultralong cycle life (maintaining 630 mAh g^{-1} at current density of 1 A g^{-1} even up to 1000 cycles). Notably, the capacity is 420 mAh g^{-1} at the high current density of 4 A g^{-1}, and can recover to the initial value when the current rate set back to 100 mA g^{-1}. To the best of our knowledge, such outstanding ultralong lifespan for $MnFe_2O_4$ or its composite have not been reported previously. All these make porous $MnFe_2O_4$ microrods promising in LIBs.

Experimental Section

Synthesis method: First, sodium bis(2-ethylhexyl) sulfosuccinate

(AOT) (1.5 mmol) was dissolved in ethylene glycol (15 ml)-H_2O (6 ml) mixtures. Then, $(NH_4)_2Fe(SO_4)_2$ (1 mmol) and $C_4H_6MnO_4{\cdot}4H_2O$ (0.5 mmol) were added into the above mixtures, as well as $Na_2C_2O_4$ (1.5 mmol) was added to another identical mixtures. The above two solutions were mingled under continuous stirring at room temperature for 9 h. Then, the pale yellow precipitate was collected and rinsed with deionized water and ethanol three times. Finally, the sample was calcined at 500 °C for 2 h in Ar atmosphere to produce $MnFe_2O_4$ microrods.

Structural characterization: X-ray powder diffraction (XRD) patterns were achieved on an advanced X-ray diffractometer (Bruker D8, $Cu_{K\alpha}$ radiation with λ = 0.1548 Å). Filed-emission scanning electron microscopy (FESEM) images and transmission electron microscopy (TEM) images were conducted on a ZEISS SUPRA^{TM}55 microscope and a JEOL JEM 1011 microscope. High-resolution transmission electron (HRTEM) images were acquired on a JEM 2100 microscope. Fourier transform infrared spectra (FTIR) in the range 4000-400 cm^{-1} were recorded on VERTEX-70 instrument, using the KBr pellet technique. Thermal gravimetric analysis (TGA) was conducted in Ar atmosphere on a Mettler Toledo TGA/SDTA851 thermal analyzer. Nitrogen adsorption/desorption isotherms were taken with a micromeritics ASAP-2020HD88 instrument.

Electrochemical measurements: Electrochemical characterization was performed in 2032 coin-type cells, which were assembled in an argon-filled glovebox (Mikrouna, Super 1220/750/900) with Li metal as the reference/counter electrode. The electrolyte was a solution of 1 M $LiPF_6$ dissolved in mixture of ethylene carbonate/diethyl carbonate/dimethyl carbonate (EC/DEC/DMC) with volume ratio of 1:1:1 and Celgard 2400 microporous membrane used as a separator. The working electrodes were prepared by $MnFe_2O_4$/acetylene black/sodium carboxyl methyl cellulose in weight ratio of 7:2:1. The mixture was dispersed in a few drops of deionized water and milled for 2h, resulting a homogeneous slurry. The slurry was then coated onto copper foil with a wetting thickness of 200 μm, and dried in the vacuum oven at 60 °C for 12 h. Disk electrodes (14 mm in diameter) were punched with the typical loading of active material ranged between 1.5 and 2.0 mg cm^{-2}. Galvanostatic cycling was conducted on Land-CT2001A battery cycler (Wuhan, China) at 25 °C. The cyclic voltammogram profiles were performed by means of a LK2005A electrochemical workstation (Tianjin China) at a scanning rate of 0.1 mV s^{-1} with 0.01 and 3.0 V as cut-off voltages.

Results and discussion

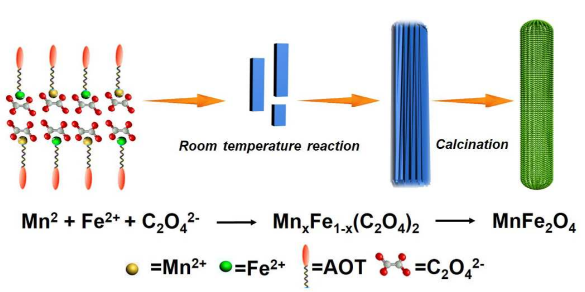

Scheme 1. Schematic illustration on the formation of porous $MnFe_2O_4$ microrods.

Scheme 1 demonstrates the fabrication process of porous $MnFe_2O_4$ microrods. According to the literature, AOT can dissolve in mixed solvents EG-H_2O forming a simple microemulsion system, which provides the way to control the size and morphology of grown crystals.[17-19] The metal ions Mn^{2+} and Fe^{2+} react with $C_2O_4^{2-}$ to form $Mn_xFe_{1-x}(C_2O_4)_2$ nucleus, as well as the anionic surfactant molecules AOT absorbed on the primary particle surface. Because of the surfactant molecules self-association during heating, primary particles aggregate into sheet-like morphology and further connect each other to form rod-like morphology by decreasing the interfacial energy.[20-22] After that, the microrods were calcinated in Ar atmosphere leading to the generation of $MnFe_2O_4$ sample. Due to the thermal stability of one dimensional structure and releasing of gases, $MnFe_2O_4$ sample basically keeps microrod structure and becomes highly porous, which would promote structure stability during lithiation/delithiation due to the pores can accommodate the volume change.

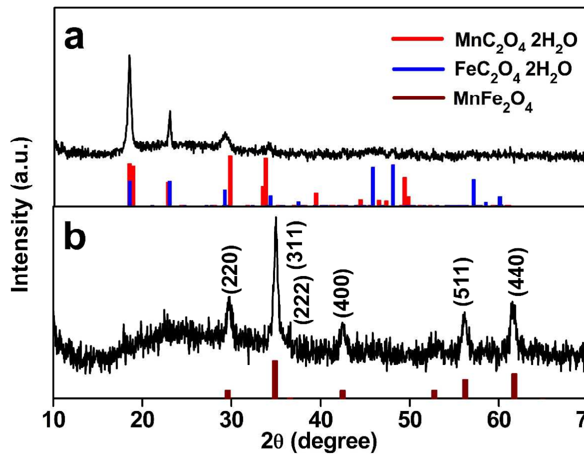

Fig. 1 XRD patterns of (a) the precursor obtained after room temperature reaction. (b) The final product after calcination process.

The crystal structure of the precursor and final product were investigated by XRD to confirm the phase transformation. As shown in Fig. 1a, all diffraction peaks can be assigned to a solid solution of $FeC_2O_4{\cdot}2H_2O$ (JCPDS Card, no. 22-0635) and $MnC_2O_4{\cdot}2H_2O$ (JCPDS Card, no. 25-0544) due to the structural similarity and close solubility. FTIR spectra (Fig. S1a) were further conducted to verify the composition of precursor. As shown in Fig. S1a, the broad band at 3377 cm^{-1} is related to the stretching vibration of –OH groups coming from molecular water or absorbed water. The bands at 1317 cm^{-1}, 1362cm^{-1} and 1619 cm^{-1} can be ascribed to symmetric stretches of –C-O and –C=O, respectively. Meanwhile, 819, 730 and 495 cm^{-1} are assigned to the bending vibrations of –C-O as well as C-C=O.[23,24] After the calcination, all the diffraction peaks in Fig. 1b can be corresponded to $MnFe_2O_4$ (JCPDS Card, no. 38-0430). No peaks of any oxalate can be observed. The crystal size is about 18 nm according to the Scherrer equation. This result is also supported by the TGA curve (Fig. S1b). There are two weight loss processes in Fig. S1b. The first one below 200 °C is attributed to the dehydration of molecular water and absorbed water, while the second one is due to the decomposition of the precursor $Mn_xFe_{1-x}C_2O_4$ accompanying with the release of gases.[25] The value of total weight loss is about 56.9%, which is agreement well with the theoretical value (57.1%). Based on the TGA curve, the calcination temperature was set at 600 °C to ensure the complete transformation of the precursor.

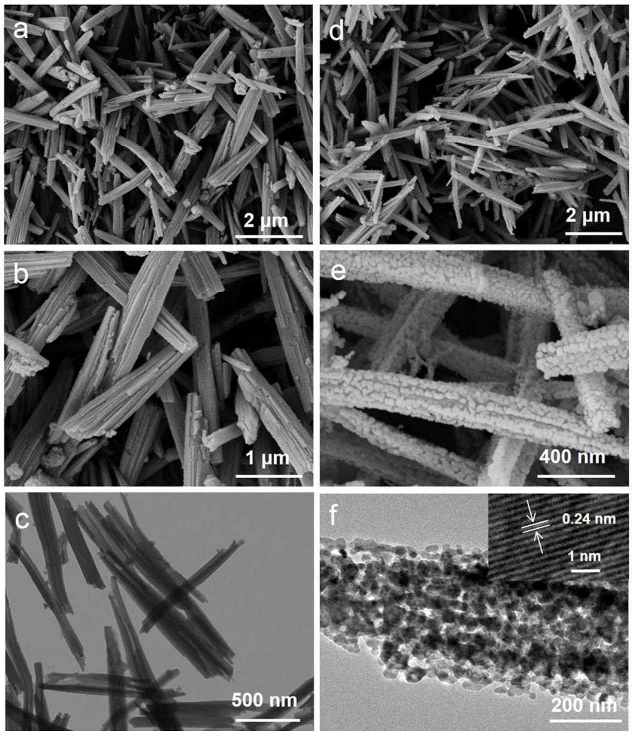

Fig. 2 SEM and TEM images of (a-c) the precursor and (d-f) the porous $MnFe_2O_4$ microrods. HRTEM image (inset of Fig. 2f).

The morphologies and structure features of the precursor and $MnFe_2O_4$ are examined by SEM and TEM (Fig. 2). The low magnification SEM image (Fig. 2a) indicates that the precursor is composed of uniform microrods with diameter of approximately 200 nm as well as length of 2~3 μm. A close up observation on the precursor reveals that these microrods composed of some stacks arranged in parallel (Fig. 2b and 2c). After calcination in Ar atmosphere for 2 h, the precursor completely changed into $MnFe_2O_4$ and basically maintained its one dimensional morphology (Fig. 2d). Nonetheless, the surface of $MnFe_2O_4$ becomes pretty rough compared with precursor because of the large weight loss during the decomposition process. As shown in Fig. 2e and 2f, the microrods seem like comprised of many nanoparticles which interconnected with each other forming the porous structure. Their porous feature can be visualized through the contrast difference in TEM image (Fig. 2f). Moreover, the primary particles size is about 20 nm, which is in consistence with the calculation from the XRD patterns. A lattice fringe with the *d*-spacing of about 0.24 nm, is corresponded to the (222) planes of $MnFe_2O_4$ crystal.

Nitrogen adsorption/desorption isotherms were performed to investigate the specific surface areas and porous nature of $MnFe_2O_4$ microrods. As shown in Fig. 3, the N_2 isotherm exhibits a typical type IV with type H1 hysteresis loop, indicating the mesoporous characteristics.[26] According to the Brunauer-Emmett-Teller (BET) model, the surface area of the porous $MnFe_2O_4$ microrods is 24.38 $m^2\ g^{-1}$, as well as the total pore volume is 0.18 $cm^3\ g^{-1}$. Based on the Barrett-Joyner-Halenda

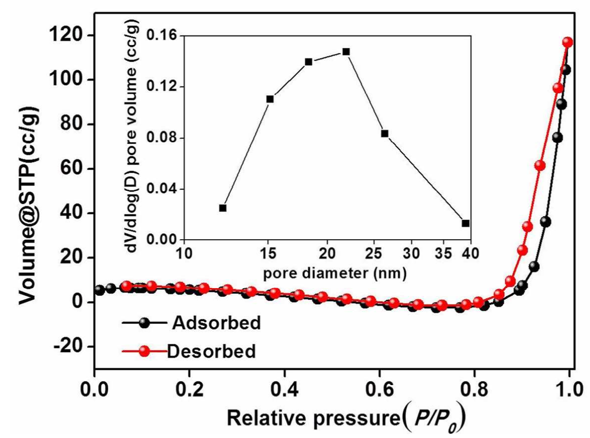

Fig. 3 N_2 adsorption/desorption isotherm of porous $MnFe_2O_4$ microrods and thecorresponding pore size distribution (inset).

(BJH) plots, the pore size is in the range of 14-35 nm, confirming the samples containing the mesopores. Such porous electrode material would benefit the better cycle lives and higher rate capabilities of lithium ion batteries, due to the pores can accommodate volume changes during cycling, facilitate charge transfer and reduce path length for ion diffusion.[14]

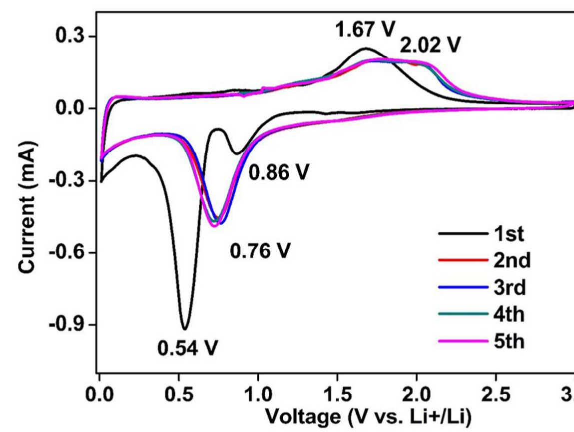

Fig. 4 Cyclic voltammongrams of the $MnFe_2O_4$ sample at a rate of 0.1 mV s^{-1} in the voltage of 0.01-3.0 V vs. Li/Li^+

The electrochemical performances of porous $MnFe_2O_4$ microrods were investigated using half cells with Li metal as a reference and counter electrode. Fig. 4 demonstrates the first five consecutive cyclic voltammetry (CV) curves of $MnFe_2O_4$ sample. During the first cathodic process, the peak around 0.86 V may be corresponded to solid electrolyte interface (SEI) layer on the electrode surface due to the electrolyte decomposition.[27] The intense peak centered at 0.54 V can be ascribed to the reduction of $MnFe_2O_4$ to metal Mn, Fe and formation of Li_2O, and which is slightly shifted to higher potentials in the following cycles that may be associated with the structure rearrangement. [7,28] Based on the in situ TEM characterization of lithiation/delithiation mechanism of $MnFe_2O_4$,[9] the anodic peak set at 1.67 V in the first cycle could be assigned to the oxidation of Mn to MnO as well as Fe to Fe_3O_4. The anodic peak became wide and positively shifted to 2.02 V in subsequent scans due to the polarization of electrode materials.[5] Remarkably, the CV curves overlap significantly upon further sweeps, illustrating that high reversible

Cite this: DOI: 10.1039/c0xx00000x

www.rsc.org/xxxxxx

ARTICLE TYPE

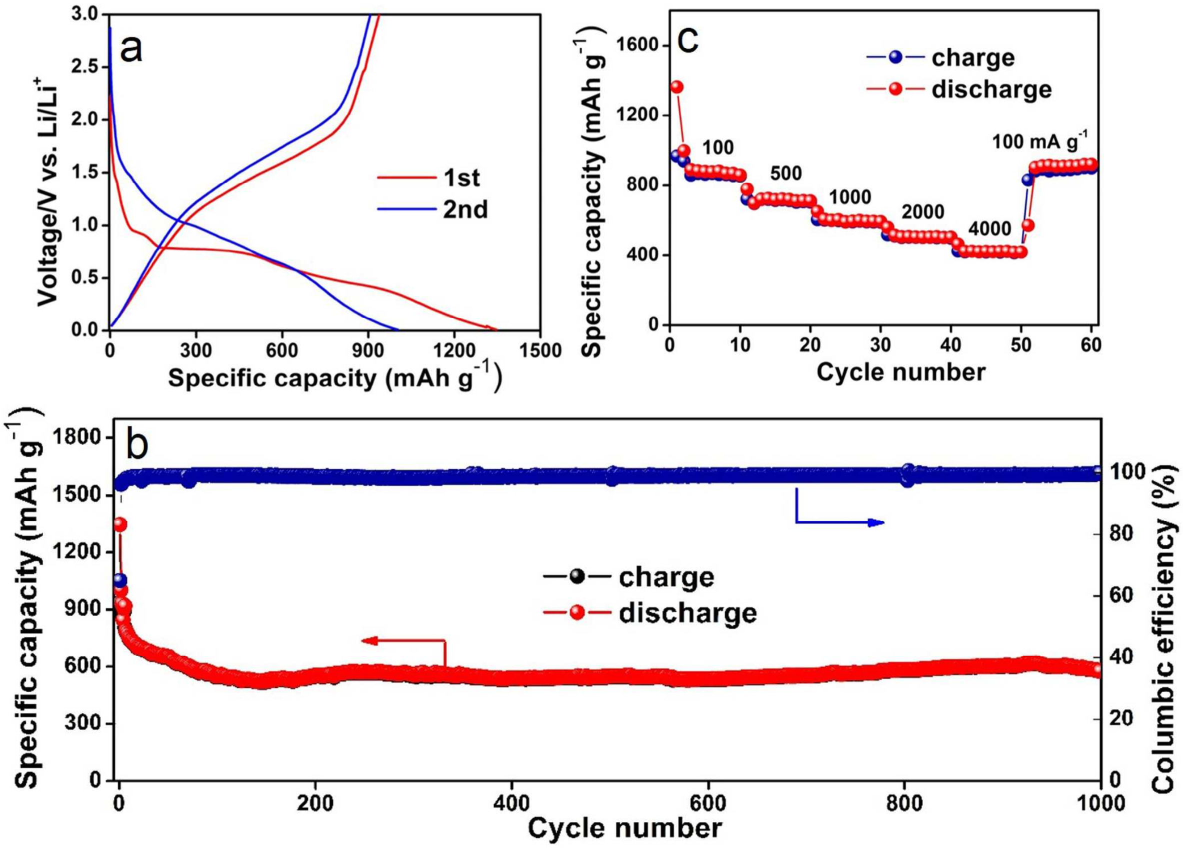

Fig. 5 (a) Voltage profiles vs. specific capacity detected at 1st cycle and 2nd cycle. (b) Charge and discharge capacity and coulombic efficiency vs. cycle number at a current density of 1 A g^{-1} up to 1000 cycles. (c) Charge and discharge capacity at different specific currents.

lithiation/delithiation once the initial structure arrangement completed and confirming the good cycling performance.

The results for galvanostatic cycling of porous $MnFe_2O_4$ microrods are presented in Fig. 5. Fig. 5a shows the voltage profiles for the first two cycles. The slope between the open-circuit voltage (2.5 V) and 0.75 V, might be the partly lithiation of $MnFe_2O_4$ and the formation of SEI.[27] The platform at about 0.75 V and the succedent slope corresponds to the reduction of $Li_xMnFe_2O_4$ along with Li_2O matrix formation. The initial discharge capacity (1336mAh g^{-1}) is significantly higher than the theoretical capacity （917 mAh g^{-1}） according to the chemical reaction ($MnFe_2O_4$ + 8Li →Mn + 2Fe + $4Li_2O$). The excess capacity is associated to the interfacial storage, lithium insertion into acetylene black along with the formation of SEI film.[27,29] A reversible specific capacity of 937 mAh g^{-1} is observed during the following delithiation process, indicating the coulombic efficiency of the first cycle is 70.1%. The relative low coulombic efficiency is attributed to the partly irreversible reaction of SEI film along with incomplete oxidation of metal particles, which is common observed in plentiful metal oxide electrodes.[6-9,27,30] In the following cycles, the coulombic efficiency maintains approximate 98%, exhibiting the good reversibility of the electrode after the fifth cycle.

Fig. 5b shows the cycling performance of the porous $MnFe_2O_4$ microrods electrodes at the current density of 1 A g^{-1}. It is noteworthy that the reversible capacity gradually reduces until it retains ~ 600 mAh g^{-1}, and then maintains at 630 mAh g^{-1} up to 1000 cycles. This phenomena is widespread in transitional metal oxides electrodes because the lithiation/delithiation process can produce the new exposed surface that might interact with the electrolyte, and generate new reversible SEI layer.[31-34] The appropriate SEI layer leads to cycling stability and long cycle performance.[35] To express the advantages of porous $MnFe_2O_4$ microrods, the cycling performance of $MnFe_2O_4$ nanorods (Figure S2 and S3) has been tested at the same current density of 1 A g^{-1}. The reversible capacity of $MnFe_2O_4$ nanorods decreased rapidly to 200 mAh g^{-1} after 300 cycles, showing bad capacity retention. The superior performance of porous $MnFe_2O_4$ microrods might be ascribed to the larger pore volume and bigger surface area promoting good access of the electrode surface to the electrolyte as well as charge transfer. The comparatively long one dimentional structure also provides continuous electron transfer channels.[12] Besides, this proformance is also better than most of the previous reports of $MnFe_2O_4$ materials.[6-9] For example, the synthesized mesoporous $MnFe_2O_4$ microspheres, it only exhibits 442 mAh g^{-1} after 50 cycles at a current density of 742.4 mA g^{-1}.[6] Later, $MnFe_2O_4$-graphene nanocomposites can reach 767 mAh g^{-1} up to 50 cycles at a current density of 1 A g^{-1}.[7] Recently, a $MnFe_2O_4$-reduced graphene oxide (rGO) nanocomposite has been obtained through a facile one-pot process (581.2 mAh g^{-1} at a current density of 1A g^{-1} after 200 cycles).[8] Meanwhile, the $MnFe_2O_4$ graphene nanosheet synthesized by Zhao *et al* presented 765 mAh g^{-1} at a current density of 1 A g^{-1} up to 100 cycles.[9]

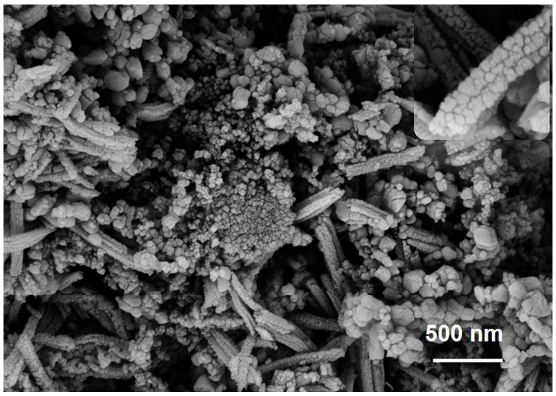

Figure 6. SEM images of $MnFe_2O_4$ electrode after the rate tests.

The high rate capability of porous $MnFe_2O_4$ microrods was also investigated upon increasing the current density every 10 cycles (Fig. 5c). Specific capacities of 890, 720, 600, 500, 420 mAh g^{-1} have been obtained at the current density of 100, 500, 1000, 2000, 4000 mA g^{-1}, respectively. The capacity is 420 mAh g^{-1} at high current density of 4 A g^{-1}, which is still much higher than the theoretical capacity of commercial graphite (372 mAh g^{-1}). Importantly, when the current rate turns back to 100 mA g^{-1}, the specific capacity of around 905 mAh g^{-1} can be retrieved, confirming that even fast charging and discharging does not influence the structure stability of the electrode significantly. As for the morphology change, SEM images of $MnFe_2O_4$ electrode after high-rate testing are shown in Figure 6. The electrode still retain one-dimensional morphology after 70 cycles upon varying current densities. In particular, $MnFe_2O_4$ electrode still remains the porous character.

The outstanding electrochemical performance of $MnFe_2O_4$ sample may be due to the uniform distribution of porous one-dimensional structure.[3,14] The well interacted pores allow for easy diffusion of the electrolyte, provides good access of the electrolyte to the material surface. Simultaneously, the open space separating neighboring particles can constrain volume expansion of active material (60% volume expansion of $MnFe_2O_4$).[9] Furthermore, the one-dimensional structure composed of nanosized particles cannot only provide extra active site for Li^+ storage, but also effectively reduce path lengths for Li^+ diffusion.[12] Noteworthy, such small feature sizes permit sufficient utilization of active materials in electrode, which may contribute to the increased capacity especially at high rates. As expected, porous $MnFe_2O_4$ microrods anode manifests excellent cyclic stability and rate capability compared to previously reported $MnFe_2O_4$-based anode materials.[6-9]

Conclusions

In summary, porous $MnFe_2O_4$ microrods are successfully synthesized by a simple process, involving room temperature precipitation to form $Mn_xFe_{1-x}(C_2O_4)_2$ microrods, and finally moderate annealing in Ar. The morphological characteristics of $MnFe_2O_4$ have been investigated by means of SEM, TEM images and N_2 adsorption/desorption isotherm. In such porous one dimensional structure, $MnFe_2O_4$ exhibits ultalong cycle lives and excellent rate capability, maintaining 630 mAh g^{-1} at current density of 1 A g^{-1} up to 1000 cycles. This work illustrates the potential of porous $MnFe_2O_4$ microrods for the design of high power LIBs, with the addition of benignity and natural abundance of manganese and iron oxides.

Acknowledgments

This work was supported by the 973 Project of China (No.2011CB935901), National Natural Science Foundation of China (Nos. 91022033, 51172076, 21471090), Shandong Provincial Natural Science Foundation for Distinguished Young Scholar (JQ201205), Independent Innovation Foundations of Shandong University (2012ZD007), and New-faculty Start-up Funding in Shandong University (No. 20111017).

Notes and references

[a]*Key Laboratory of Colloid and Interface Chemistry, Ministry of Education, School of Chemistry and Chemical Engineering, Shandong University, Jinan 250100, China. Email:* qianyt@sdu.edu.cn.
[b]*Hefei National Laboratory for Physical Science at Microscale and Department of Chemistry, University of Science and Technology of China, Hefei, 230026, China*
† Electronic Supplementary Information (ESI) available: IR spectras and TGA curves. See DOI: 10.1039/b000000x/

1 M. Armand and J.M. Tarascon, Nature, 2008, **451**, 652.
2 Y. Idota, T. Kubota, A. Matsufuji, Y. Maekawa and T. Miyasaka, Science, 1997, **276**, 1395.
3 P. G. Bruce, B. Scrosati and J. M. Tarascon, *Angew. Chem. Int. Ed.*, 2008, **47**, 2930.
4 P. Poizot, S. Laruelle, S. Grugeon, L. Dupont and J. M. Tarascon, *Nature*, 2000, **407**, 496.
5 H. B. Wu, J. S. Chen, H. H. Hng and X. W. Lou, *Nanoscale*, 2012, **4**, 2526.
6 Z. L. Zhang, Y. H. Wang, Q. Q. Tan, Z. Y. Zhong, F. B. Su, *J. Colloid Interface Sci.*, 2013, **398**, 185.
7 Y. L. Xiao, J. T. Zai, L. Q. Tao, B. Li, Q. Y. Han, C. Yu and X. F. Qian, *Phys. Chem. Chem. Phys.*, 2013, **15**, 3939.
8 H. Tang, P. B. Gao, A. Xing, S. Tian, Z. H. Bao, *RSC Adv.*, 2014, **4**, 28421.
9 S. Y. Liu, J. Xie, Q. M. Su, G. H. Du, S. C. Zhang, G. S. Cao, T. J. Zhu and X. B. Zhao, *Nano Energy*, 2014, **8**, 84.
10 K. Zhang, X. P. Han, Z. Hu, X. L. Zhang, Z. L. Tao and J. Chen, *Chem. Soc. Rev.*, 2015, **44**, 699.
11 N. N. Wang, H. Y. Xu, L. Chen, X. Gu, J. Yang and Y. T. Qian, *J. Power Sources*, 2014, **247**, 163.
12 J. Y. Huang, L. Zhong, C. M. Wang, J. P. Sullivan, W. Xu, L. Q. Zhang, S. X. Mao, N. S. Hudak, X. H. Liu, A. Subramanian, H. Y. Fan, L. Qi, A. Kushima and J. Li, *Science*, 2010, **330**, 1515.
13 Z. C. Bai, N. Fan, C. H. Sun, Z. C. Ju, C. L. Guo, J. Yang and Y. T. Qian, *Nanoscale*, 2013, **5**, 2442.
14 A. Vu, Y. Q. Qian and A. Stein, *Adv. Energy Mater.*, 2012, **2**, 1056.
15 Z. C. Bai, X. Y. Zhang, Y. W. Zhang, C. L. Guo and B. Tang, *J. Mater. Chem. A*, 2014, **2**, 16755.

16 N. N. Wang, L. Chen, X. J. Ma, J. Yue, F. E. Niu, H. Y. Xu, J. Yang and Y. T. Qian, *J. Mater. Chem. A*, 2014, **2**, 16847.
17 J. H. Fendler, *Chem. Rev.*, 1987, **87**, 877.
18 J. Tanori and M. P. Pileni, *Langmuir*, 1997, **13**, 639.
19 D. Chen, G. Z. Shen, K. B. Tang, Z. H. Liang and H. G. Zheng, *J. Phys. Chem. B*, 2004, **108**, 11280.
20 H. Cölfen and M. Antonietti, *Angew. Chem. Int. Ed.*, 2005, **44**, 5576.
21 H. Cölfen and S. Mann, *Angew. Chem. Int. Ed.*, 2003, **42**, 2350.
22 L. Zhou, H. B. Wu, T, Zhu and X. W. Lou, *J. Mater. Chem.*, 2012, **22**, 827.
23 N. Mancilla, V. Caliva, M. C. D'Antonio, A. C. González-Baró and E. J. Baran, *J. Raman Spectrosc.*, 2009, **40**, 915.
24 D. P. Wang, I. Belharouak, G. W. Zhou and K. Amine, *J. Electrochem. Soc.*, 2013, **160**, A3108.
25 W. W. Zhou, K. B. Tang, S. Y. Zeng and Y. X. Qi, *Nanotechnology*, 2008, **19**, 065602.
26 M. Kruk and M. Jaroniec, *Chem. Mater.*, 2001, **13**, 3169.
27 S. Laruelle,S. Grugeon, P. Poizot, M. Dollé, L. Dupont and J. M. Tarascon, *J. Electrochem. Soc.*, 2002, **149**, A627.
28 G. Binotto, D. Larcher, A. S. Prakash, R. Herrera Urbina, M. S. Hegde and J. M. Tarascon, *Chem. Mater.*, 2007, **19**, 3032.
29 P. Balaya, H. Li, L. Kienle and J. Maier, *Adv. Funct. Mater.*, 2013, **13**, 621.
30 S. Grugeon,S. Laruelle, R. Herrera-Urbina, L. Dupont, P. Poizot and J. M. Tarascon, *J. Electrochem. Soc.*, 2001, **148**, A285.
31 S. Grugeon,S. Laruelle, L. Dupont and J. M. Tarascon, *Solid State Sci*, 2003, **5**, 895.
32 J. S. Do and C. H. Weng, *J. Power Sources*, 2005, **146**, 482.
33 G. M. Zhou, D. W. Wang, F. Li, L. L. Zhang, N. Li, Z. S. Wu, L. Wen, G. Q. Lu and H. M. Cheng, *Chem. Mater.*, 2010, **22**, 5306.
34 X. L. Sun, C. L. Yan, Y. Chen, W. P. Si, J. W. Deng, S. Oswald, L. F. Liu and O. G. Schmidt, Adv. Energy Mater., 2013, DOI: 10.1002/aenm.201300912
35 H. T. Sun, G. Q. Xin, T. Hu, M. P. Yu, D. L. Shao, X. Sun and J. Lian, *Nat. Commun.*, 2014, DOI: 10.1038/ncomms5526.

Table of contents

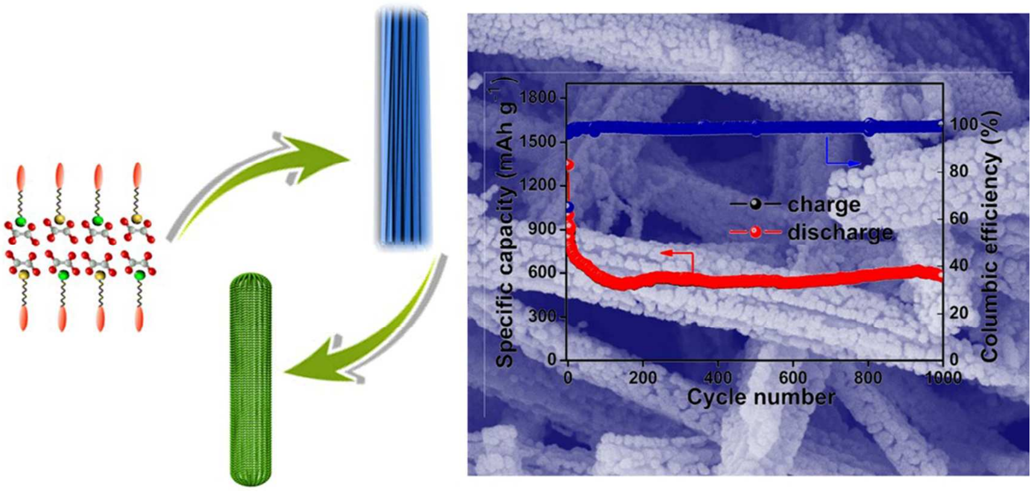

Porous $MnFe_2O_4$ microrods exhibit 630 mAh g^{-1} after 1000 cycles at 1 A g^{-1} and high coulombic efficiency (> 98%).